Atomic Crystal and Molecular Dynamics Simulation Structures of Human Carbonic Anhydrase II: Insights into the Proton Transfer Mechanism[†,‡]

S. Zoë Fisher,[§,▽] C. Mark Maupin,[||,▽] Monika Budayova-Spano,[⊥] Lakshmanan Govindasamy,[§] Chingkuang Tu,[#] Mavis Agbandje-McKenna,[§] David N. Silverman,[§,#] Gregory A. Voth,*[,||] and Robert McKenna*[,§]

Department of Biochemistry and Molecular Biology, College of Medicine, University of Florida, Gainesville, Florida 32610, Center for Biophysical Modeling and Simulations and Department of Chemistry, University of Utah, Salt Lake City, Utah 84112, EMBL Grenoble-Outstation, 6 Rue Jules Horowitz BP156, 38042 Grenoble, France, and Department of Pharmacology and Therapeutics, College of Medicine, University of Florida, Gainesville, Florida 32610

Received December 1, 2006; Revised Manuscript Received December 21, 2006

ABSTRACT: Human carbonic anhydrase II (HCA II) is a zinc-metalloenzyme that catalyzes the reversible interconversion of CO_2 and HCO_3^-. The rate-limiting step of this catalysis is the transfer of a proton between the Zn-bound solvent molecule and residue His64. In order to fully characterize the active site structural features implicated in the proton transfer mechanism, the refined X-ray crystal structure of uncomplexed wild type HCA II to 1.05 Å resolution with an R_{cryst} value of 12.0% and an R_{free} value of 15.1% has been elucidated. This structure provides strong clues as to the pathway of the intramolecular proton transfer between the Zn-bound solvent and His64. The structure emphasizes the role of the solvent network, the unique positioning of solvent molecule W2, and the significance of the dual conformation of His64 in the active site. The structure is compared with molecular dynamics (MD) simulation calculations of the Zn-bound hydroxyl/His64$^+$ (charged) and the Zn-bound water/His64 (uncharged) HCA II states. A comparison of the crystallographic anisotropic atomic thermal parameters and MD simulation root-mean-square fluctuation values show excellent agreement in the atomic motion observed between the two methods. It is also interesting that the observed active site solvent positions in the crystal structure are also the most probable positions of the solvent during the MD simulations. On the basis of the comparative study of the MD simulation results, the HCA II crystal structure observed is most likely in the Zn-bound water/His64 state. This conclusion is based on the following observations: His64 is mainly (80%) orientated in an inward conformation; electron density omit maps infer that His64 is not charged in an either inward or outward conformation; and the Zn-bound solvent is most likely a water molecule.

Carbonic anhydrases (CAs)[1] are ubiquitous metalloenzymes, present throughout virtually all living organisms, including animals, plants, algae, bacteria, and archaebacteria. They catalyze the reversible hydration of carbon dioxide to bicarbonate and a proton and, therefore, are involved in a vast number of physiological processes linked to respiration, acid−base homeostasis, photosynthesis, and other biosynthetic pathways. Humans express at least 14 CA isozymes (HCA I−XIV) with varying catalytic activity and cellular distribution (*1*, *2*). HCA II is the most extensively studied of these isozymes because it has widespread tissue distribution with large amounts located in red blood cells, where it is involved in respiration, and because it is among the most efficient of the HCAs with a catalytic turnover rate of 10^6 s^{-1} (*3*).

The CA mechanism can be split into the two steps depicted below (eqs 1 and 2) (*4*−*6*). In the hydration direction, the first step is the binding of CO_2 in a hydrophobic region of the active site, followed by the nucleophilic attack by a Zn-bound hydroxyl on the substrate carbon to form HCO_3^-. The HCO_3^- is then readily displaced from the active site by H_2O (eq 1).

$$CO_2 + EZnOH^- \rightleftharpoons EZnHCO_3^- \overset{H_2O}{\rightleftharpoons} EZnH_2O + HCO_3^- \quad (1)$$

$$\text{His64-}EZnH_2O + B \rightleftharpoons H^+\text{His64-}EZnOH^- + B \rightleftharpoons \text{His64-}EZnOH^- + BH^+ \quad (2)$$

The second part of the reaction is rate-limiting in the maximum velocity and involves the intra and intermolecular

† This work was supported by grants GM25154 (to D.N.S. and R.M.) and GM53148 (to G.A.V.) from the National Institutes of Health and the Maren Foundation (to R.M.).

‡ The atomic coordinates have been deposited in the Protein Data Bank with entry 2ILI.

* To whom correspondence should be addressed: Phone: (352)-392-5696. Fax: (352) 392-3422. E-mail: rmckenna@ufl.edu (R.M.). Phone: (801)581-7272. Fax: (801) 581-4353. E-mail: voth@chem.utah.edu (G.A.V.).

§ Department of Biochemistry and Molecular Biology, University of Florida.

|| University of Utah.

⊥ EMBL Grenoble-Outstation.

Department of Pharmacology and Therapeutics, University of Florida.

▽ S.Z.F. and C.M.M. contributed equally to this work.

1 Abbreviations: CAs, carbonic anhydrases; HCA II, human carbonic anhydrase II; MD, molecular dynamics; RMSF, root mean square fluctuation; rmsd, root mean square deviation; PMF, potential of mean force.

10.1021/bi062066y CCC: $37.00 © 2007 American Chemical Society
Published on Web 02/24/2007

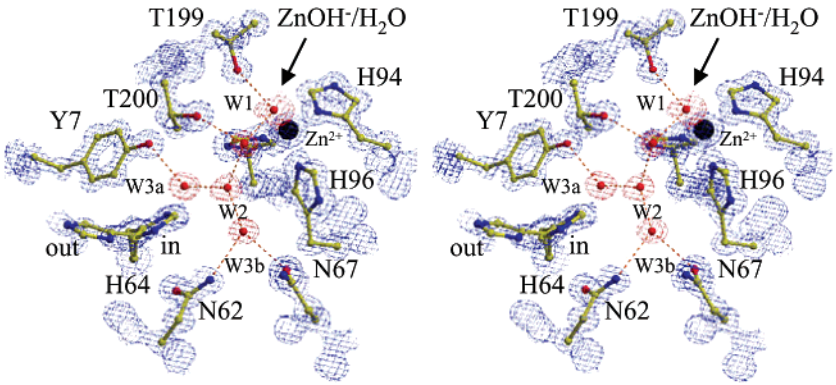

FIGURE 1: Stereoview of the active site of HCA II. Ball-and-stick representation of the active site residues are as labeled, and the zinc atom and waters are shown as black and red spheres, respectively. The inferred hydrogen bonds are indicated as dashed red lines. The $2F_o - F_c$ electron density map is depicted as a blue or red mesh and contoured at 2 σ for the side chains and the solvent and at 3 σ for the zinc. The Figure was generated and rendered with BobScript and Raster3D (*30*, *31*).

transport of a proton. The intramolecular proton transport occurs between the Zn-bound solvent and the side chain of His64, which is located on the edge of the active site, where the proton is further transferred out to the bulk solvent (eq 2). The mutation of His64 to an alanine (H64A HCA II) reduces the proton transfer activity 10- to 50-fold (*7*). Various crystal structures, determined at different pH values, have revealed that His64 occupies dual conformations, the so-called "in", pointing inward toward the active site, and "out", pointing outward away from the active site, and it is thought that the apparent flexibility of His64 is essential to its function as an efficient proton shuttle (Figure 1) (*8*, *9*).

In the active site of HCA II, there are several amino acids (Tyr7, Asn62, Asn67, Thr199, and Thr200) that participate in coordinating a well-ordered solvent network (W1, W2, W3a, and W3b) between the Zn-bound solvent and His64 (Figure 1). Thr199 forms a hydrogen bond with the Zn-bound solvent, which, in turn, is hydrogen bonded to W1. W1 is further stabilized by Thr200 and the next solvent in the chain, W2. The solvent network then branches as W2 is hydrogen bonded to both W3a and W3b. W3a is further coordinated by the hydroxyl group of Tyr7, whereas W3b is stabilized by Asn62 and Asn67. This solvent network has been previously shown to be conserved over a broad pH range (pH 5.0−10.0) and localizes W2, W3a, and W3b all in close proximity to His64, when in the inward conformation (Figure 1) (*9*).

There are several high resolution (∼1.0 Å) crystal structures of HCA II available; however, these are either of the H64A HCA II mutant complexed with a chemical proton transfer rescuer (*10*) or of the wild type HCA II in complex with inhibitors (*11*).

Hence, in an effort to observe the wild type HCA II active site without being perturbed by either the kinetic rescuer or the inhibitor present, the crystal structure of HCA II alone to 1.05 Å resolution has been determined and refined. This structure is discussed in terms of the active site residues and solvent organization and what the structural details imply to their participation in the proton transfer mechanism of HCA II. These observations are then further compared with molecular dynamics (MD) simulation calculations of various intermediate states of HCA II to provide insight into what the most probable functional state of the enzyme is as observed in the crystalline state.

EXPERIMENTAL PROCEDURES

HCA II Purification and Crystallization. Wild type HCA II was expressed in *Eschericia coli* BL21 pLysS (DE3) cells and purified as described elsewhere (*12*, *13*). The purified protein was buffer exchanged into 50 mM Tris-Cl at pH 8.2 by dialysis prior to concentration. The protein was concentrated to ∼25 mg/mL with Amicon Ultra centrifugation filtration devices with a molecular weight cutoff of 10 kDa. The final concentration of HCA II was determined from the molar absorptivity at 280 nm (5.5×10^4 M^{-1} cm^{-1}). Crystals were grown at 277 K with the hanging drop vapor diffusion method using 5 μL of protein solution and 5 μL of precipitant (100 mM Tris-Cl at pH 7.8 and 1.15 M sodium citrate) suspended over a 1000 μL precipitant reservoir.

X-ray Data Collection and Processing. Crystals appeared within 7 days and were cryoprotected prior to data collection by quick-dipping them in a 20% glycerol precipitant solution (v/v). High-resolution X-ray synchrotron diffraction data at 100 K were collected on a Quantum 210 CCD detector system at the European Synchrotron Radiation Facility (ESRF) (beamline ID29) using a wavelength of 1.0052 Å. Three different crystals were used for data collection with a 0.5° oscillation angle and an exposure time of 1 s at 75 mm crystal-to-detector distances. A total of 360 images (180° data) were recorded that yielded a total of 522,157 reflections measured to 1.05 Å resolution. Diffraction data were recorded beyond 1.0 Å resolution, but because it was very sparse at the corners of the detector, it was not included in data processing. Data processing was performed using DENZO, and data were scaled and reduced with SCALEPACK (*14*). The final data set was merged to 98,392 independent reflections with an overall R_{symm} of 0.079. The data set statistics for each resolution shell are given in Table 1.

Crystallographic Refinement Procedure. The phases for structure determination were obtained using molecular replacement methods with the software package, Crystallography and NMR Systems (CNS), version 1.1 (*15*). The crystal structure of perdeuterated HCA II (PDB accession code: 2AX2) (*16*) was used as the search model with the zinc and solvent removed to avoid model bias. A random set of 5% of unique reflections were set aside for the calculation of R_{free}. Initial refinement using data from 20.0−

Table 1: Data Set Statistics for Each Resolution Shell

resolution (Å)	unique reflections	redundancy	completeness (%)	R_{symm}[a]
20.0 − 2.85	5672	2.0	97.8	0.052
2.85 − 2.26	5541	2.9	97.6	0.060
2.26 − 1.98	5459	3.0	96.7	0.061
1.98 − 1.80	5408	3.8	96.0	0.069
1.80 − 1.67	5385	3.8	95.4	0.080
1.67 − 1.57	5298	3.8	94.8	0.098
1.57 − 1.49	5296	3.9	94.0	0.115
1.49 − 1.42	5232	3.9	93.6	0.138
1.42 − 1.37	5215	3.8	93.0	0.168
1.37 − 1.32	5165	3.8	92.4	0.197
1.32 − 1.28	5130	3.8	92.0	0.246
1.28 − 1.24	5131	3.8	91.5	0.262
1.24 − 1.21	5088	3.8	90.7	0.295
1.21 − 1.18	5037	2.7	90.2	0.254
1.18 − 1.16	4995	1.9	89.3	0.152
1.16 − 1.13	5017	1.9	89.4	0.181
1.13 − 1.11	4830	1.9	86.9	0.204
1.11 − 1.09	4081	1.8	73.4	0.256
1.09 − 1.07	3052	1.8	54.2	0.296
1.07 − 1.05	2360	1.8	42.5	0.404
total	98392	3.1	87.6	0.079

[a] $R_{symm} = \Sigma\ |I - \langle I\rangle|/\Sigma\langle I\rangle$.

2.0 Å started with one cycle of rigid body refinement and annealing by heating to 3000 K with gradual cooling. This was followed by geometry restrained position refinement and temperature factor refinement. At this point $F_o - F_c$ Fourier electron density omit maps were generated, and these maps clearly showed the position of the zinc and active site solvent, which were subsequently built into their respective density. This was followed by more position and temperature factor refinement until the *R* factors converged. Next, the general (nonactive site) solvent was added to the model using the automated water picking routine as implemented in CNS. A total of 456 water molecules were added iteratively until no more could be found at the 2 σ cutoff level. The initial structure refinement concluded with position and temperature factor refinement and yielded and R_{work} and R_{free} values of 0.216 and 0.235, respectively (Table 2).

Refinement to 1.05 Å resolution continued using SHELXL97 in the conjugate-gradient least-squares (CGLS) mode with SHELXL default restraints used for the protein geometry (*17*, *18*). After the first round of 15 cycles of CGLS, the R_{work} and R_{free} values decreased to 0.168 and 0.192, respectively. $2F_o - F_c$ and $F_o - F_c$ maps were generated, and the model and solvent molecules were manually inspected using the molecular graphics program Coot (*19*). These maps revealed dual conformations for seven amino acid side chains (Ile22, Asp34, His64 (the proton shuttle residue), Asp175, Glu187, Ser217, and Ser220). These residues were built accordingly and included in the model. Because of the high resolution and data/parameter ratio (~9:1), this was followed by a full anisotropic refinement. After the anisotropic refinement, one round of 15 cycles of CGLS were followed by the manual inspection of new electron density maps and placement of more solvent. Badly placed and poorly refined solvent (that were not visible in $2F_o - F_c$ maps contoured at 1.5 σ and/or had *B* factors larger than 50 Å^2) were also removed at this point. Following the addition of more solvent, another round of 15 cycles of CGLS with anisotropic refinement was done. At this point,

Table 2: Refinement Protocol

cycle	description	step	R_{work} (%)[a]	R_{free} (%)[b]	resolution (Å)
		CNS			
1	rigid body	starting model without solvent/Zn	36.1	36.9	20.0 − 2.00
	annealing		32.6	34.9	
2	minimize	Zn, active site HOH placed	32.4	34.8	20.0 − 1.05
	B individual		27.7	29.5	
3	minimize		25.6	27.0	
	B individual		24.4	25.6	
4	water pick	456 HOH added	22.1	23.7	
5	minimize	manual adjustments	21.8	23.8	
	B individual		21.6	23.5	
		SHELXL			
1	CGLS 15	dual conformers	16.8	19.2	
2	CGLS 15	full anisotropic	12.3	15.8	
3	CGLS 15	add HOH	12.3	15.8	
4	CGLS 15	remove bad HOH	12.3	15.8	
5	CGLS 15	add HOH, anisotropic	11.9	15.1	
6	CGLS 20	riding hydrogens and final manual adjustments	12.0	15.1	
	CGLS 5				

[a] $R_{work} = \Sigma\ |F_o| - |F_c|/\Sigma\ |F_{obs}| \times 100$. [b] R_{free} is calculated in the same manner as R_{work}, except that it uses 5% of the reflection data omitted from refinement.

Table 3: Refinement and Final Model Statistics

resolution (Å)	20.0−1.05
[a]R_{cryst} (%)	12.0
[b]R_{free} (%)	15.1
no. of residues/atoms	3 − 261/2092[c]
no. of water molecules	337
rmsd bond lengths (Å)	0.004
rmsd bond angles (°)	1.400
Ramachandran statistics (%) most favored/additionally allowed	88/12
B factors (Å^2) main chain/side chain/Zn/solvent	11.3/15.5/5.3/28.9

[a] $R_{cryst} = \Sigma\ |F_o| - |F_c|/\Sigma\ |F_{obs}| \times 100$. [b] R_{free} is calculated in same manner as R_{cryst}, except that it uses 5% of the reflection data omitted from refinement. [c] Including atoms for residues Ile22, Asp34, His64, Asp175, Glu187, Ser217, and Ser220 with dual conformations.

protein H atoms were included at calculated positions but were explicitly excluded for active site residues Tyr7, Asp62, His64, Asp67, Thr199, and Thr200 (Figure 1). Final model adjustments were performed followed by 5 cycles of CGLS with a resultant convergence of R_{cryst} and R_{free} to 0.120 and 0.151, respectively. The model geometries and statistics were analyzed by PROCHECK and Moleman (*20*, *21*). All data refinement steps and final model statistics are given in Tables 2 and 3.

Molecular Dynamics Procedures. Three systems were used to study the solution structure of the hydration and dehydration reaction in HCA II. Because this study has been described in the next article (*22*), only a brief description of this work is given here. The initial starting coordinates for the MD simulations were taken from the wild type HCA II crystal structure (PDB accession code 2CBA, including the 220 solvent molecules) (*23*), and placed in a solvated cubic simulation box ($L \approx 75$ Å). The dehydration reaction was modeled only with the Zn-bound hydroxyl/His64$^+$ with

Table 4: Distances between Active Site Residues and Water Molecules

	distance (Å)
Zn: Zn-bound solvent	1.80
W_{OD}: T199 (N)	3.07
Zn-bound solvent: T199 (OG1)	2.95
Zn-bound solvent: W1	2.66
W1: T200 (OG1)	2.78
W1: W2	2.75
W2: W3a	2.76
W2: W3b	2.73
W3a: Y7 (OH)	2.77
W3b: N62 (ND2)	3.00
W3b: N67 (OD1)	2.70
W2, W3a, W3b: H64[a] (ND1)	3.33, 3.30, 3.71

[a] His64 is the inward conformer.

His64 in the outward orientation because the inward orientation for His64 exhibited a low occurrence at equilibrium. Whereas for the hydration reaction, the Zn-bound water/His64 system was modeled with His64 in both the inward and outward orientations because a prevalence of both orientations was observed at equilibrium (*22*).

RESULTS

The crystals of wild type HCA II diffracted X-rays to higher than 1.0 Å resolution; however, there was not enough data collected in the outer shells to be included in the refinement. The overall data were 87.6% complete (42.5% in the highest resolution shell) from 20.0 to 1.05 Å resolution and had an R_{symm} of 0.079 (0.404 in the highest resolution shell) (Table 1). The data was isomorphous with other HCA II crystal structures and had unit cell dimensions of $a = 42.21$, $b = 41.29$, and $c = 72.15$ Å, and $\beta = 104.39°$. The final refined model had good geometry with root-mean-square deviations (rmsd) for bond lengths and angles of 0.004 Å and 1.4°, respectively. The average B values for the main chain and side chain atoms were 11.3 and 15.5 Å^2, respectively. The variation of the residue-average B values versus residue number is shown in Figure S1 (Supporting Information). A total of 337 solvent molecules were added to the model with an average B value of 28.9 Å^2 (Table 3). The final refined model had an R_{cryst} of 12.0% and an R_{free} of 15.1%. Superposition of the structure onto the structure of wild type HCA II to 1.5 Å resolution (pdb accession code 2AX2) (*16*) gave an rmsd for all C-α atoms of 0.16 Å. Data, refinement steps, and final model statistics are given in Tables 1−3.

The overall active site details of HCA II at high resolution are, not surprisingly, similar to those of previously determined lower resolution structures, for example, PDB accession codes 2CBA (*8*);1TEQ (*9*); and 2AX2 (*16*). The refined distances between amino acid side chains and the oxygen of solvent molecules within the active site are summarized in Table 4. What does appear to be apparent, which was not in the lower resolution studies, is that the solvent molecule W2 (which is the only ordered solvent molecule in that active site stabilized exclusively by other solvent molecules) is trigonally hydrogen bonded with equal distance (2.75 ± .02 Å) by W1, W3a, and W3b. In addition, within this cluster of solvent molecules, only W2 is in the plane of the imidazole ring of His64 when in the inward conformation (Figures 1 and 2). Also, the higher resolution refinement provides more

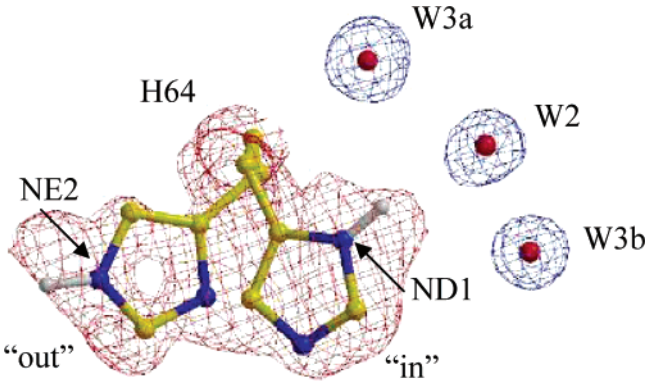

FIGURE 2: Inward and outward conformations of His64. Ball-and-stick representation of His64 as labeled, and waters are shown as red spheres. The His64 $F_o - F_c$ omit electron density map is depicted as a red mesh and contoured at 2.5 σ. The solvent $2F_o - F_c$ electron density map is depicted as a blue mesh and contoured at 2.0 σ. The location of putative hydrogen atoms are as shown. The Figure was generated and rendered with BobScript and Raster3D (*30, 31*).

detail on the interactions of ND1 of His64 in the inward conformation. From the refinement, it appears that only W2 and W3a seem to be in close enough proximity to form weak hydrogen bonds with His64 (both 3.3 Å), whereas W3b is somewhat further away (3.7 Å) and, therefore, unlikely to contribute to any direct stabilizing effect on His64 (Table 4; Figures 1 and 2). The explicit removal of hydrogens prior to riding hydrogen refinement and the subsequent omit maps generated for active site residues Tyr7, Asp62, Asp67, Thr199, and Thr200 did not reveal convincing additional densities that could correspond to hydrogen atoms. This might be expected because these residues are exposed to the solvated active site cavity, but most had refined B factors <10 Å^2 and may imply that some of these side chains are ionized, pointing into the active site to stabilize the solvent structure.

However, the Zn-bound solvent, which had a refined B factor of 8.5 Å^2, did reveal features not previously observed in lower resolution structures. Close inspection of the omit electron density maps (contoured at 4.5 σ) in the proximity of the Zn-bound oxygen O_Z were interpreted to be two hydrogen atoms, H1 and H2, as shown in Figure 3. On the basis of the hydrogen positions, the Zn-bound solvent was modeled as a water molecule (H1-O_Z-H2) with standard geometry. The coordinates of the fitted water were taken from the neutron diffraction structure of endothiapepsin (PDB accession 1GKT) (*24*). The Zn-bound water molecule was modeled with H1 forming a linear hydrogen bond to the solvent molecule O_{DW} (Figure 3). This well-ordered water molecule has been previously observed in other HCA II structures and is termed deep water. It is thought that CO_2 binding in this hydrophobic region (Val121, Val 143, Leu198, and Trp209) in the active site displaces this solvent molecule (O_{DW}) that is hydrogen bonded to the amide group of Thr199 (*23*). With the Zn-bound water in this orientation, the other hydrogen atom H2 is not directly hydrogen bonded, it is exposed and pointing away from the zinc. It is plausible that during catalysis and subsequent O_{DW} displacement, the Zn-bound water can undergo a small rotation that places H2 in a position for transfer to W1. This would leave a hydroxyl bound to the zinc, consistent with the catalytic mechanism (eqs 1 and 2).

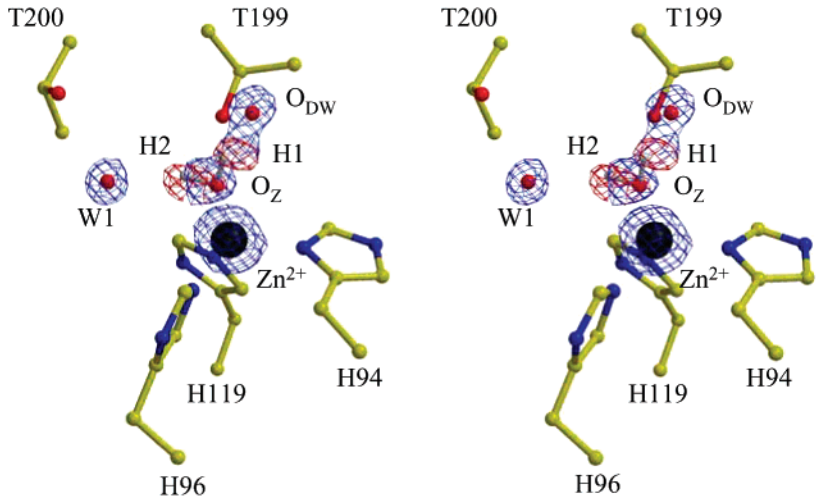

FIGURE 3: Stereoview of the zinc-bound solvent and coordinating ligands. The $2F_o - F_c$ electron density map is depicted as a blue mesh contoured at 2.0 σ (showing nonhydrogen atoms), and the $F_o - F_c$ electron density map is depicted as a red mesh and contoured at 4.5 σ (showing the putative position of two hydrogens, H1 and H2). The hydrophobic residues V121, V143, L198, and W209 that surround the deep water O_{WD} are not shown for clarity. The Figure was generated and rendered with BobScript and Raster3D (*30*, *31*).

An alternate interpretation of this density is that Oz-H1 and O_{DW}-H2 represent two hydroxyls located near the zinc. However, this is unlikely because the distance between O_{DW} and H2 is $\sim$ 1.4 Å and thus too long for an O−H bond.

His64, the proton shuttle residue, sits on the edge of the active site cavity where it has access to the solvent network in the active site as well as the bulk solvent outside the enzyme. In this study, a more accurate view has emerged as to the relative occupancies of the inward and outward orientations of His64. During the final stages of refinement, the two His64 conformers were removed from the model, and a $F_o - F_c$ omit map was calculated (Figure 2). An inspection of this map contoured at 2.5 σ visually demonstrated the relative density contribution of each conformation but also showed additional density that could possibly correspond to hydrogen atoms (H_{ND1} in the inward and H_{NE2} in the outward conformation) and, therefore, provide putative information that the imidazole rings are both uncharged, but the site of the hydrogen atom has moved from ND1 in the inward to NE2 in the outward conformation. The hydrogens shown in Figure 2 are constrained by standard geometry. With this geometry, the hydrogen H_{ND1} in the inward conformation forms an almost linear (170°) hydrogen bond (2.4 Å) with W2. However, the placement of hydrogen H_{NE2} in the outward position is less convincing and is brought about by the low occupancy and exposure to the bulk solvent of His64 (Figure 2).

In the final structural refinement to obtain the same relative *B* factors for the atoms of the imidazole side chains in the two conformations, the occupancy was set at 80% inward (χ_1 and χ_2 are 47 and 99°, respectively) and 20% outward (χ_1 and χ_2 are −55 and 111°, respectively) (Figure 2). It should be noted that in the final refined model, no additional residual $F_o - F_c$ electron density was observed near the NE2 in the inward or ND1 in the outward His64 conformation (data not shown). This implies that these nitrogens do not have hydrogen atoms within the imidazole rings and, therefore, supports the observation that His64 in both conformations was uncharged.

Interestingly, the electron density maps clearly showed the orientation of His64 in both the inward and outward conformations to have similar χ_2 torsion angles. This is not surprising because rotation about χ_2 is limited because plausible steric clashes with surrounding amino acids Trp5 and Asn62 would occur without them also moving, and there is no evidence from the electron density maps or the anisotropic refined atomic thermal *B* factors of Trp5 and Asn62 demonstrating conformational movement. Hence, these observations would imply that His64 is only able to undergo a simple rocking motion with approximately 100° of rotational freedom about χ_1 from the in-to-out conformation (Figures 1 and 2).

The calculated MD simulation potential of mean force (PMF) for the orientation of His64 in the Zn-bound water/His64 and the Zn-bound hydroxyl/His64$^+$ systems are plotted (Figure 3 in ref 22 (*22*)). The relative distributions of the inward and outward orientations for the Zn-bound water/His64 can be directly compared to $F_o - F_c$ Fourier maps to help explain the dual conformation densities for His64 (Figure 2).

The MD PMF for Zn-bound water/His64 showed that the transition of His64 flipping from the inward to the outward positions occurred at $\chi_1 = -7°$, with an energy barrier for rotation of 5.6 kcal mol^{-1}, and for the Zn-bound hydroxyl/His64$^+$ the transition state occurred at $\chi_1 = 17°$, with an energy barrier of 6.2 kcal mol^{-1}. (Figure 3 in ref 22 (*22*)). The MD results show that the inward orientation is favored in the Zn-bound water/His64 state, whereas the outward orientation is favored for the Zn-bound hydroxyl/His64$^+$ state. Integration of the PMF for the Zn-bound water/His64 state of His64 shows an 86% and 14% occurrence for the inward and outward conformations, respectively. However, the Zn-bound hydroxyl/His64$^+$ state showed a 97% outward orientation and only a 3% chance of occupying the inward orientation (*22*). This clearly shows that in the Zn-bound hydroxyl/His64$^+$, the state from which proton transfer proceeds in the dehydration direction, His64 prefers the outward orientation, whereas in the Zn-bound water/His64, the state from which proton transfer proceeds in the hydration direction, His64 prefers the inward conformation.

In addition, unbiased MD simulations were conducted for the inward and outward orientation of His64 for the Zn-

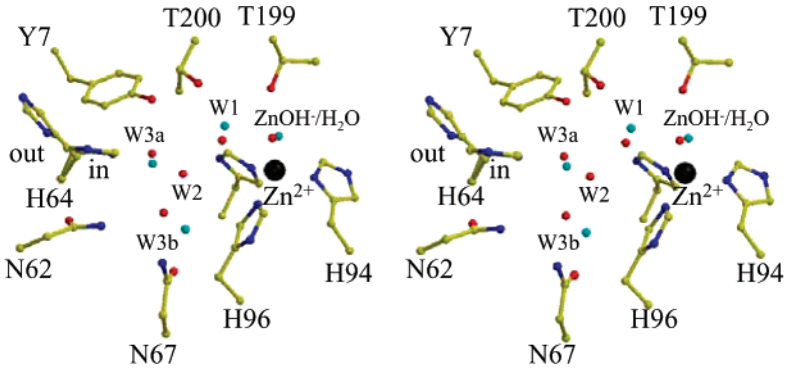

FIGURE 4: Stereoview of the active site solvent. Structural overlay of the refined crystallographic solvent and MD simulation distribution of solvent molecule occurrences for the Zn-bound water/His64 inward trajectories. Ball-and-stick representation of the active site residues are as labeled, with the zinc atom shown as black sphere. The crystallographic solvent positions are depicted as red spheres and the positions of the highest solvent occurrences in the simulation as blue spheres. The Figure was generated and rendered with BobScript and Raster3D (*30*, *31*).

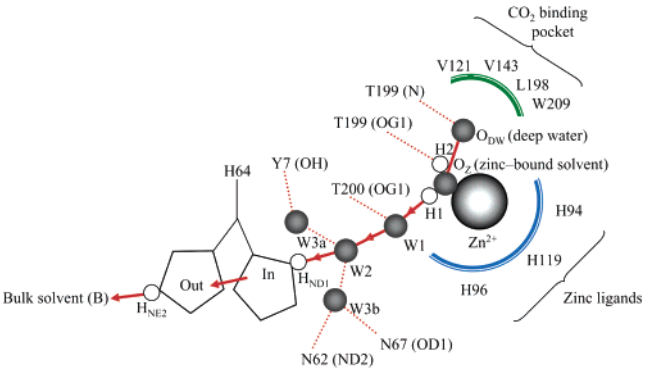

FIGURE 5: Proposed proton transfer pathway. Shown are the geometry and interactions of the active site amino acids and solvent arrangement of HCA II. The large black, small black, and open white circles represent the zinc, solvent oxygen, and hydrogen atoms, respectively. The inward and outward conformations of His64 are depicted as open pentagons, and the hydrogen atom positions are as labeled. The Zn-bound (H1-Oz-H2) and deep (O_{DW}) water are also labeled. The proposed proton transfer pathway steps are marked with red arrows. Additional, stabilizing hydrogen bonds are shown as red dashed lines. The zinc coordinating histidines and hydrophobic CO_2 pocket are shown as open blue and green curved lines, respectively.

bound water/His64 state. Given below are the MD distribution-weighted averages for the active site solvent positions (Figure 4). The Zn to Zn-bound solvent (2.02 ± 0.09 Å) and the Zn-bound solvent to Thr199 (OG1) (3.0 ± 0.1 Å) distances were direct measurements and, therefore, expected to mimic the crystal structure because of the explicit bonds between these atoms (Table 4). The MD distances between the nonexplicit solvent W3b to Asn67 (OD1) (2.84 Å) and W3b to Asn62 (ND2) (2.85 Å) were also in close agreement with the crystal structure (Table 4 and Figure 5). The MD simulation results suggest that Asn62 may be more mobile and adopt multiple conformation states in response to the motion of His64 (data not shown; *22*). Further analysis into the role of Asn62 and Asn67 would be useful to investigate their respective roles in the stabilization of the water networks and catalysis by HCA II. What is clear from these comparative studies is that the MD simulation solvent positions are consistent with the crystal structure with surprising accuracy (Figure 4).

The root-mean-square fluctuation (RMSF) results for the C-α atoms for the MD simulations shown in Figure S1 (Supporting Information) are the probability-weighted values for the Zn-bound water/His64 state in both the inward and outward orientations. These RMSF values are a measure of the flexibility of amino acids and, therefore, are comparable to the crystallographic thermal *B* factor (Figure S1, Supporting Information). The zinc−ligand histidines show the least motion, and this rigidity of the active site is probably essential for the maintenance of the proper geometry that supports catalysis. In contrast, moderate RMSF values were observed for residues Thr199 (which stabilizes the Zn-bound solvent), Thr200 (which stabilizes W1), and His64. These are most likely higher because they respond to the changing active site solution environment during catalysis. Although Tyr7 is also involved with the solvent network, it has an even higher RMSF value than the active site residues described above. However, this could be due to its proximity to the highly disordered N-terminus.

DISCUSSION

The direct comparison of the refined crystallographic thermal *B* values and the MD RMSF values show great correlation (Figure S1, Supporting Information). The agreement of these two methods for determining atomic fluctuations was first described by Post et al. for lysozome (*25*). In the case of HCA II, both show the thermal stability of the core 10 strand *β*-motif, a more moderate elevated motion in the coil and α-helical regions, and the highest thermal motion in the N- and C-termini. These two independently determined functions, representing structural motion in the crystal and solution states, correlate well with each other, even to the level of individual residues. The arrows in Figure S1 (Supporting Information) highlight this point by indicating two regions of moderate motion identified between the *β*D and E strands in both methods. This agreement between the two methods highlights that the results from the MD simulations (*22*, *25*) can be used to complement and add information to the crystallographic observations and vice versa.

The MD values for the Zn-bound water/His64 inward trajectories were also used to calculate an active site solvent probability density function, plotting the distribution of solvent molecule occurrences in the active site. This highlighted four significant regions (10 times greater than the average distribution) where the solvent was present most often, and these mapped to the positions of the Zn-bound solvent, W1, W3a, and W3b observed in the crystal structure

but not W2 (Figure 4). The Zn-bound solvent is expected to mimic the crystal data because of the explicit bonds between these atoms in the MD calculations, whereas the other solvents do not have explicit bonds between them. This is interesting because it also demonstrates how the two methods have shown comparable results, in this case the location of the most static solvent in the active site. What is of particular note is that W2 was not one of these local regions of high solvent occurrence, and this would imply that in the MD calculations, this region demonstrates greater solvent variability than in the crystal state. Perhaps this implies that W2 is a kinetically trapped hydronium ion intermediate of the proton transfer process and can only be observed in the crystal structure (Figure 4).

On the basis of the agreements drawn from both the MD and the crystallography results, a comparative study of the different MD simulations indicates that the crystalline HCA II structure observed is the Zn-bound water with an uncharged His64. This is drawn from the following observations in the crystal structure: His64 is mainly (80%) orientated in an inward conformation; electron density omit maps infer that His64 has a single hydrogen (uncharged) in both conformations (Figure 2); and the Zn-bound solvent is most likely a water molecule (Figure 3).

An analysis of the catalyzed reaction by HCA II at steady state and chemical equilibrium has led to a model of its mechanism of action that implicates two ionizing groups in the active site that have pK_a values near 7 (*4*, *6*, *26*). One of these groups corresponds to the Zn-bound H_2O, which ionizes to an OH^- and is responsible for the interconversion of CO_2 and HCO_3^- (eq 1 and Figure 3), whereas the other group, His64, is charged when involved in the transfer of a proton to the bulk solvent (eq 2 and Figure 2) (*7*).

In this study, the Zn-bound oxygen O_Z is interpreted as a putative water molecule (H1-O_Z-H2). The hydrogen H1 forms a hydrogen bond (O_Z-H1-O_{DW}; 165°, 2.4 Å) with O_{DW} (Figure 3). The hydrogen H2 does not appear involved in any interactions. However, it is possible that a small structural perturbation would orientate H2 to form a hydrogen bond with W1. In such an event, the proton H2 on the Zn-bound solvent could be transferred onward to W1 and out of the active site (eq 2 and Figure 5).

The pK_a of the Zn-bound solvent is 7.0, and the crystallization pH in this study (pH 7.8) would mean that the Zn-bound solvent in the active site is a hydroxyl. However, it is difficult to determine the ionization state of titratable groups in a crystal, and this value may be very different from that in solution. Previously, Amiss and Gurman have reported EXAFS measurements of the Zn−solvent distance in HCA I and showed over a wide pH range that the distance was 1.82 ± 0.02 Å and that this was consistent with a Zn-bound hydroxyl (*27*). However, other studies using EXAFS to investigate the Zn-bound hydroxyl and water distances showed them to be between 1.85−2.00 Å (*28*). On the basis of these findings, it is difficult to decide on measured experimental distance alone whether the Zn-bound solvent is OH^- or H_2O.

Numerous crystal structures of HCA II show that His64 occupies two distinct conformations, the in and out conformations (Figure 1), and this has been observed over a wide pH range (*8*, *9*). The proximity of His64 to the solvent network, apparent flexibility, and studies involving mutagenesis and kinetic measurements are all consistent with His64 acting as a proton shuttle by picking up a proton when it is in the inward position, moving to the outward position, and transferring it to an acceptor in the bulk solvent (Figure 5) (*7*−*9*). To date, it has been uncertain as to which of the active site waters, W2, W3a, or W3b, is correctly poised to donate/accept a proton from His64 because the solvent network leading to His64 is branched with any of the three solvent molecules, W2, W3a, and W3b, in close proximity to His64 (Figure 1).

The geometry and putative hydrogen atom, H_{ND1}, of His64 in the inward conformation has provided clues to show that W2 is the most probable water molecule that satisfies this proton transfer role. This is because W2 is the only one of this cluster of three waters to lie in the plane of the imidazole ring of His64 and is in close enough proximity to make an almost linear hydrogen bond (ND1-H_{ND1}-W2; 170°, 3.3 Å) with W2 (Table 4; Figure 2). It would appear that W3a and W3b have a more supportive role in coordinating W2 for its interaction with His64. Thus, His64 is uncharged when in the inward position and interacts with W2 (Figure 5).

Possibly, the outward conformer of His64 also has a single hydrogen atom at NE2 and is most likely also uncharged. This conformation exhibits lower occupancy of the imidazole side chain, thus making the assignment of a hydrogen atom less certain (Figure 2). This is consistent with the outward conformation NE2 of His64 being completely exposed to the bulk solvent, which would not be the case for the ND1 position. Again, at the pH of crystallization, it would be expected that His64 is uncharged (*4*). Consistent with this, the $F_o - F_c$ density shows additional density for one of the nitrogens of the imidazole side chain in both orientations.

In summary, this data suggests that His64 is uncharged in both the inward and outward conformations in the crystalline state as described in this study. The inward conformer interacts specifically with W2 via ND1 (Figures 2 and 5). This implies that although there is branching in the solvent network, the solvent molecules W3a and W3b play a supportive role for W2 to permit proton transport from the Zn-bound solvent to His64. Hence, we propose that the proton transfer from the Zn-bound water proceeds via the following pathway: Zn-H_2O → W1 → W2 → "in" His64-(ND1) → "out" His64(NE2) → B, where B is the bulk solvent (eq 2 and Figure 5). These structural features are consistent with the measured catalytic efficiency of HCA II, and computational results from Cui and Karplus that show two intervening waters between a proton donor and acceptor as the most efficient way to transfer a proton (*29*).

ACKNOWLEDGMENT

We thank William Shepard for help and support during the X-ray data collection at the ESRF (beamline ID29) and John Domsic for assistance with figures.

SUPPORTING INFORMATION AVAILABLE

A comparison of the refined crystallographic thermal *B* values versus MD simulation RMSF values for HCA II is given in Figure S1. This material is available free of charge via the Internet at http://pubs.acs.org.

REFERENCES

1. *The Carbonic Anhydrases: New Horizons* (Chegwidden,W. R., Carter, N. D., and Edwards, Y. H., Eds.) Birkhäuser Verlag, Basel, Switzerland.
2. Duda, D. M., and McKenna, R. (2004) *Handbook of Metalloproteins* (A. Messerschmidt, A., Ed.) pp 249−263, John Wiley & Sons, New York.
3. Khalifah, R. G. (1971) The carbon dioxide hydration activity of carbonic anhydrase, *J. Biol. Chem. 246*, 2561−2573.
4. Silverman, D. N., and Lindskog, S. (1988) The catalytic mechanism of carbonic anhydrase: implications of a rate-limiting protolysis of water, *Acc. Chem. Res. 21*, 30−36.
5. Christianson, D. W., and Fierke, C. A. (1996) Carbonic anhydrase: evolution of the zinc binding site by nature and by design, *Acc. Chem. Res. 29*, 331−339.
6. Lindskog, S. (1997) Structure and mechanism of carbonic anhydrase, *Pharmacol. Ther. 74*, 1−20.
7. Tu, C. K., Silverman, D. N., Forsman, C., Jonsson, B. H., and Lindskog, S. (1989) Role of histidine 64 in the catalytic mechanism of human carbonic anhydrase II studied with a site-specific mutant, *Biochemistry 28*, 7913−7918.
8. Nair, S. K., and Christianson, D. W. (1991) Unexpected pH-dependent conformation of His64, the proton shuttle of carbonic anhydrase II, *J. Am. Chem. Soc. 113*, 9455−9458.
9. Fisher, Z., Hernandez Prada, J. A., Tu, C. K., Duda, D., Yoshioka, C., An, H., Govindasamy, L., Silverman, D. N., and McKenna, R. (2005) Structural and kinetic characterization of active-site histidine as a proton shuttle in catalysis by human carbonic anhydrase II, *Biochemistry 44*, 1097−1105.
10. Duda, D. M., Govindasamy, L., Agbandje-McKenna, M., Tu, C. K., Silverman, D. N., and McKenna, R. (2003) The refined atomic structure of carbonic anhydrase II at 1.05 Å resolution: Implications of chemical rescue of proton transfer, *Acta Crystallogr., Sect. D 59*, 93−104.
11. Jude, K. M., Banerjee, A. L., Haldar, M. K., Manokaran, S., Roy, B., Mallik, S, Srivastava, D. K., and Christianson, D. W. (2006) Ultrahigh resolution crystal structures of human carbonic anhydrase I and II complexed with "two-prong" inhibitors, *J. Am. Chem. Soc. 128*, 3011−3018.
12. Khalifah, R. G., Strader, D. J., Bryant, S. H., and Gibson, S. M. (1977) Carbon-13 nuclear magnetic resonance probe of active-site ionizations in human carbonic anhydrase, *Biochemistry 16*, 2241−2247.
13. Tanhauser, S. M., Jewell, D. A., Tu, C. K., Silverman, D. N., and Laipis, P. J. (1992) T7 expression vector optimized for site-directed mutagenesis using oligodeoxyribonucleotide cassettes, *Gene 117*, 113−117.
14. Otwinowski, Z., and Minor, W. (1997) Processing of x-ray diffraction data collected in oscillation mode, *Methods Enzymol. 276*, 307−326.
15. Brünger, A. T., Adams, P. D., Clore, G. M., DeLano, W. L., Gros, P., Grosse-Kuntsleve, R. W., Jiang, J. S., Kuszewski, J., Nilges, M., Pannu, N. S., Read, R. J., Rice, L. M., Simonson, T., and Warren, G. L. (1998) Crystallography & NMR system: A new software suite for macromolecular structure determination, *Acta Crystallogr., Sect. B 54*, 905−921.
16. Budayova-Spano, M., Fisher, S. Z., Dauvergne, M. T., Agbandje-McKenna, M., Silverman, D. N., Myles, D. A. A., and McKenna, R. (2006) Production and X-ray crystallographic analysis of fully deuterated human carbonic anhydrase II, *Acta Crystallogr., Sect. F 62*, 6−9.
17. Sheldrick, G. M., and Schneider, T. R. (1997) SHELXL: high-resolution refinement, *Methods Enzymol. 277*, 319−343.
18. Engh, R. A., and Huber, R. (1991) Accurate bond and angle parameters for X-ray protein structure refinement, *Acta Crystallogr., Sect.* A *47*, 392−400.
19. Emsley, P., and Cowtan, K. (2004) Coot: model-building tools for molecular graphics, *Acta Crystallogr., Sect. D 60*, 2126−2132.
20. Laskowski, R. A., MacArthur, M. W., Moss, D. S., and Thornton, J. M. (1993) PROCHECK: a program to check the stereochemical quality of protein structures, *J. Appl. Crystallogr. 26*, 283−291.
21. Kleywegt, G. J. (1992) Moleman, unpublished program, Uppsala University, Uppsala, Sweden.
22. Maupin C. M., and Voth G. A. (2007) Preferred orientations of His-64 in human carbonic anhydrase II, *Biochemistry* 46, 2938−2947.
23. Håkansson, K., Carlsson, M., Svensson, L. A., and Liljas, A. (1992) Structure of native and apo carbonic anhydrase II and structure of some of its anion-ligand complexes, *J. Mol. Biol. 227*, 1192−1204.
24. Coates, L., Erskine, P. T., Wood, S. P., Myles, D. A. A., and Cooper, J. B. (2001) A neutron Laue diffraction study of endothiapepsin: Implications for the aspartic proteinase mechanism, *Biochemistry 40*, 13149−13157.
25. Post, C. B., Brooks, B. R., Karplus, M., Dobson, C., Artymiuk, P. J., Cheetham, J. C., and Phillips, D. C. (1986) Molecular dynamics simulations of native and substrate-bound lysozyme, *J. Mol. Biol. 190*, 455−479.
26. Steiner, H., Jonsson, B. H., and Lindskog, S. (1975) The catalytic mechanism of carbonic anhydrase: hydrogen isotope effects on the kinetic parameters of the human C isoenzyme, *Eur. J. Biochem. 59*, 253−259.
27. Amiss, J. C., and Gurman, S. J. (1999) Biological EXAFS at room temperature, *J. Synchrotron Radiat. 6*, 387−388.
28. Bergquist, C., Fillebeen, T., Morlok, M. M., and Parkin, G. J. (2003) Protonation and reactivity towards carbon dioxide of the mononuclear tetrahedral zinc and cobalt hydroxide complexes, [Tp(Bu)t(,Me)]ZnOH and [Tp(Bu)t(,Me)]CoOH: comparison of the reactivity of the metal hydroxide function in synthetic analogues of carbonic anhydrase, *J. Am. Chem. Soc. 125*, 6189−6199.
29. Cui, Q., and Karplus, M. (2003) Is a "proton wire" concerted or stepwise? A model study of proton transfer in carbonic anhydrase, *J. Phys. Chem. B 107*, 1071−1078.
30. Esnouf, R. M. (1997) An extensively modified version of MolScript that includes greatly enhanced coloring capabilities, *J. Mol. Graphics Modell. 15*, 132−134.
31. Merritt, E. A., and Bacon, D. J. (1997) Raster3D: photorealistic molecular graphics, *Methods Enzymol. 277*, 505−524.

BI062066Y